Buckling of a stiff film bound to a compliant substrate (part III). Herringbone solutions at large buckling parameter

Basile Audoly

Institut Jean le Rond d'Alembert, UMR 7190 du CNRS,
CNRS/Université Pierre et Marie Curie, 4 place Jussieu, F-75252 Paris Cedex 05

Arezki Boudaoud

Laboratoire de Physique Statistique, UMR 8550 du CNRS/Paris 6/Paris 7
École normale supérieure, 24 rue Lhomond, F-75231 Paris Cedex 05

Abstract

We study the buckling of a compressed thin elastic film bonded to a compliant substrate. An asymptotic solution of the equations for a plate on an elastic foundation is obtained in the limit of large residual stress in the film. In this limit, the film's shape is given by a popular origami folding, the Miura-ori, and is composed of parallelograms connected by dihedral folds. This asymptotic solution corresponds to the herringbone patterns reported previously in experiments: the crests and valleys of the pattern define a set of parallel, sawtooth-like curves. The kink angle obtained when observing these crests and valleys from above are shown to be right angles under equi-biaxial loading, in agreement with the experiments. The absolute minimum of energy corresponds to a pattern with very slender parallelograms; in the experiments, the wavelength is instead selected by the history of applied load.

Key words: Buckling, Plates, Thermal stress, Asymptotic analysis, Energy methods

1 Introduction

The buckling of multi-layered materials is relevant to the formation of wrinkles in human skin, to the templating and assembly of materials (see e. g. Genzer and Groenewold, 2006, for a review), and to the design of sandwich

panels (Allen, 1969). A thin metallic film deposited on an elastomer provides a simple multi-layer geometry investigated experimentally by Bowden et al. (1998); Huck et al. (2000); Yoo et al. (2002). When the system cools down after deposition, compressive residual stress is induced in the film by the large thermal expansion coefficient of the substrate, relative to that of the film. This residual stress can lead to film buckling into straight wrinkles (Bowden et al., 1998), observable as a set of parallel stripes, especially near defects or boundaries. Here we focus on the herringbone patterns, also known as chevrons; the crests and valleys of the herringbone follow zigzag paths. Herringbone patterns are observed at moderate to large residual stress, as shown in the pictures in Chen and Hutchinson (2004) after Bowden et al. (1998); Huck et al. (2000). Numerical simulations of these patterns have been performed by Chen and Hutchinson (2004) and Huang et al. (2005).

In the first companion paper (Audoly and Boudaoud, 2007a), we investigated the stability of straight wrinkles, also called straight stripes, and showed that the they become unstable towards *undulating* stripes by a secondary instability. In the second companion paper (Audoly and Boudaoud, 2007b), we solved a simplified buckling model and found that the undulating stripes evolve smoothly towards a pattern similar to herringbones under increasing load; these approximate solutions feature sharp folds along crests and valleys, like herringbones, but these crests and valleys have sinusoidal shapes instead of zigzag ones. The goal of the present paper is to show that this approximate solution, applicable to arbitrary loads, can be improved in the case of large load by an asymptotic solution of the full equations for plates on an elastic foundation, with no approximation. This exact solution describes herringbone patterns, with zigzag folds, in agreement with former experiments and numerical simulations reported in the literature.

Our solution is inspired by the similarity of the herringbone pattern with origami folding of a piece of paper, as first described by Miura (1980). The relevance of Miura-ori folding to herringbone buckling has been alluded to by Chen and Hutchinson (2004); Mahadevan and Rica (2005) but has not been exploited so far. Here, we construct minimizers of the energy of the system at large buckling parameter; these minimizers are based on the Miura-ori construction, which provides a family of developable shapes. We derive the energy and geometrical properties of these solutions. A similar technique for building solutions in the limit of a large parameter, by asymptotic analysis, has been used by Choksi et al. (1999); Conti (2000) for ferromagnetic materials and by Pomeau and Rica (1997); Jin and Sternberg (2001) for the compression of free standing elastic plates. Applications of these methods to the theory of elastic shells are reviewed in the book by Libai and Simmonds (1998).

This series of papers addresses the buckling of an elastic plate on an elastic foundation. In this paper, we focus on the limit of large residual stress in
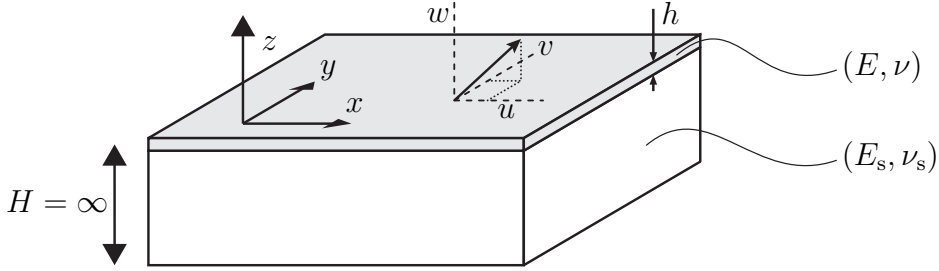
Fig. 1. Geometry of the problem and notations.

the film. In Section 2, we recall the formulation of the problem given in the companion papers. In Section 3, we discuss the case of developable solutions having curvilinear ridges, like those obtained in the second companion paper (Audoly and Boudaoud, 2007b), and show that their energy is minimized by going to zigzag ridges. The main results are presented in Section 4, where we investigate in detail developable solutions comprising zigzag crests and valleys connected by piecewise straight ridges, as in the popular origami folding due to Miura (Miura-ori).

2   Formulation

The film is assumed to be infinitely long in its two in-plane directions, x and y. We start by writing the elastic energy of the system per unit area; we remain in the framework of Hookean elasticity and assume a linearly elastic response — although some geometric nonlinearities will be considered for the plate. The film is loaded with a biaxial, uniform differential strain. We consider the case of compressive residual stress in the film, for which the planar configuration is potentially unstable by buckling. We do not consider delamination: buckling can occur without delamination when the film is much stiffer than the substrate. The film is described by the Föppl–von Kármán equations for plates undergoing moderate deflections (Timoshenko and Gere, 1961). The foundation is assumed to be an infinitely deep solid with a linear response.

2.1   Film

Let E, ν and h be Young's modulus E, Poisson's ratio and thickness of the film. The film is loaded with a compressive differential strain η_x, η_y, the x and y directions being chosen as the principal directions of this strain (see Fig. 1 for the geometry and notations). The loading parameters η_x and η_y, assumed to be homogeneous along the film, are taken positive in the case which we consider, namely when the film is in compression. The residual stress in the film is related to this differential strain by the constitutive relations for plane

3

stress elasticity:

$$\sigma^0_{xx} = -\frac{E\,(\eta_x + \nu\,\eta_y)}{1-\nu^2} \qquad \text{and} \qquad \sigma^0_{yy} = -\frac{E\,(\nu\,\eta_x + \eta_y)}{1-\nu^2}. \tag{1}$$

When film buckles so as to relax this residual stress, the in-plane strain (in actual configuration) is given by

$$\epsilon_{xx} = -\eta_x + \frac{\partial u}{\partial x} + \frac{1}{2}\left(\frac{\partial w}{\partial x}\right)^2, \tag{2a}$$

$$\epsilon_{xy} = \frac{1}{2}\left(\frac{\partial u}{\partial y} + \frac{\partial v}{\partial x} + \frac{\partial w}{\partial x}\frac{\partial w}{\partial y}\right), \tag{2b}$$

$$\epsilon_{yy} = -\eta_y + \frac{\partial v}{\partial y} + \frac{1}{2}\left(\frac{\partial w}{\partial y}\right)^2. \tag{2c}$$

This strain tensor uses the planar, stress-free configuration of the film as a reference. Here $u(x,y)$ and $v(x,y)$ are the two components of the in-plane displacements, along x and y respectively, and $w(x,t)$ is the out-of-plane displacement (deflection). Using the classical approximations of the Föppl-von Kàrmàn plate theory, nonlinearities in the in-plane displacement (u,v) have been neglected, although those involving the deflection w are retained.

The detailed formulation for the elastic energy of the film can be found in the companion papers (Audoly and Boudaoud, 2007a,b). Here we will only use the decomposition of the film energy into a stretching part $\mathcal{E}_{fs}$ and bending one $\mathcal{E}_{fb}$,

$$\mathcal{E}_f = \mathcal{E}_{fs} + \mathcal{E}_{fb}. \tag{3}$$

All energies noted with the letter $\mathcal{E}$ are counted per unit area, unlike those written with the letter $\mathcal{U}$. The stretching modulus is proportional to Eh while the bending one is proportional to Eh^3: the bending stiffness goes to zero much faster in the limit of a small thickness h, which we consider here. This property can be used for asymptotic analyses (see e.g. Ben Amar and Pomeau, 1997; Lobkovsky, 1996; Pomeau and Rica, 1997; Jin and Sternberg, 2001).

2.2   Substrate

The elastic foundation, which fills the half-space $z < 0$ in the undeformed configuration, has Young's modulus E_s and Poisson's ratio ν_s. Introducing the Fourier transform of the film deflection,

$$\hat{w}(k_x, k_y) = \int \mathrm{d}x\,\mathrm{d}y\; w(x,y)\exp[-i(k_x x + k_y y)], \tag{4}$$

the energy of the substrate, which has a linear response by assumption, can be written as

$$\mathcal{E}_{\mathrm{s}} = \frac{1}{L_x L_y} \int \mathrm{d}k_x \, \mathrm{d}k_y \, E_{\mathrm{s}}^* \sqrt{k_x^2 + k_y^2} \, \hat{w}(k_x, k_y)\hat{w}(-k_x, -k_y). \tag{5}$$

It depends on the effective modulus E_{s}^*, which is Young's modulus E_{s} multiplied by a function of Poisson's ratio ν_{s}, as explained in the companion paper (Audoly and Boudaoud, 2007a):

$$E_{\mathrm{s}}^* = \frac{E_{\mathrm{s}} \, (1 - \nu_{\mathrm{s}})}{(1 + \nu_{\mathrm{s}}) \, (3 - 4\nu_{\mathrm{s}})}. \tag{6}$$

2.3 Optimization problem

The goal of the paper is to derive equilibrium solutions describing buckled states. This involves minimizing the total energy, which is the sum of the film and substrate energies:

$$\mathcal{E}_{\mathrm{t}}(\{u, v, w\}) = \mathcal{E}_{\mathrm{s}}(\{w\}) + \mathcal{E}_{\mathrm{f}}(\{u, v, w\}). \tag{7}$$

Here, curly braces mean that the energy is a function, *i. e.* depends on the values of the functions $u(x, y)$, $vx(, y)$ and $w(x, y)$ over the entire domain. The energy has to be minimized with respect to these three components

$$(u(x, y), v(x, y), w(x, y))$$

of the film displacement, at fixed material parameters and differential strain (η_x, η_y).

3   Developable solutions with ridges

In this paper, we consider the limit of a large buckling parameter $\eta_x \gg 1$ and $\eta_y \gg 1$. Then, the out-of-plane displacement is many times the thickness of the film. In this limit, the bending energy of the film becomes much smaller than that of stretching, because the stretching stiffness becomes comparatively very large. As a consequence, the film attempts to relax stretching and the optimal shape has a vanishing strain tensor $\epsilon_{\alpha\beta}$ (by convention, Greek indices run over the in-plane directions, x and y). Then, the center surface is called [1] developable (Spivak, 1979). More accurately, the solution is developable almost

---

[1] More accurately, the displacement defines an isometric embedding. This is what we mean in the following by 'developable'.

everywhere, except along internal 'boundary layers' which form a network of ridges and conical points (Lobkovsky, 1996; Ben Amar and Pomeau, 1997). As a matter of fact, we have already encountered developable solutions in the limit of a large load (Audoly and Boudaoud, 2007b): using an simplified buckling model, we showed in the companion paper that the film profile converges to developable shapes comprising ridges.

3.1 Film deflection

We seek solutions to the equations for a stiff film on an elastic foundation in the form of periodic, developable surfaces. A classical result in the differential geometry of surfaces is that developable surfaces are always ruled, *i. e.* are spanned by straight lines called generatrices (Spivak, 1979) — however, not all ruled surfaces are developable. The cylindrical pattern (straight stripes) shown in Fig. 2a is a ruled surface (the generatrices of which are all parallel). However, these generatrices are also parallel to the mean plane of the film and, as a result, this pattern does not relax residual compression in the direction of the stripes: it is not developable in the sense that it does not satisfy $\epsilon_{\alpha\beta} = 0$ for α, $\beta = x, y$. Indeed, a necessary condition for a film profile to be developable ($\epsilon_{\alpha\beta} = 0$) can be derived by averaging equation (2c) over the film area

$$\eta_y = \frac{1}{2} \left\langle \left(\frac{\partial w}{\partial y} \right)^2 \right\rangle, \tag{8}$$

where $\langle \cdot \rangle$ denotes an average. To derive the equation above, we have used $\langle v \rangle = 0$ since $v(x, y)$ is a bounded function, and the film dimensions are infinite. Equation (8) shows that if a generatrix of the film lies above a line in the plane (Oxy) parallel to the direction y, this generatrix has to be tilted with respect to the plane (x, y), that is $\partial w/\partial y \neq 0$, in order to relax the initial longitudinal strain $\eta_y \neq 0$ — this property can easily be extended to generatrices having an arbitrary orientation, not necessarily parallel with the y axis when projected in plane.

Therefore, developable surfaces comprise tilted generatrices. On the other hand, the film is bonded to the substrate and the deflection $w(x, y)$ has to remain bounded — otherwise, the energy of the substrate would be infinite. This shows that the limit shape of the film, which is developable, cannot remain smooth: the straight generatrices cannot be tilted with respect to the plane (Oxy) while remaining at a finite distance from it. More specifically, this suggests the geometrical construction in Fig. 2, whereby a cylindrical profile, initially tilted with respect to the mean plane of the film, undergoes repeated mirror symmetries and is patched to form a periodic, developable surface with curvilinear ridges. This pattern is enclosed between two planes $\mathcal{P}_+$ and $\mathcal{P}_-$

6
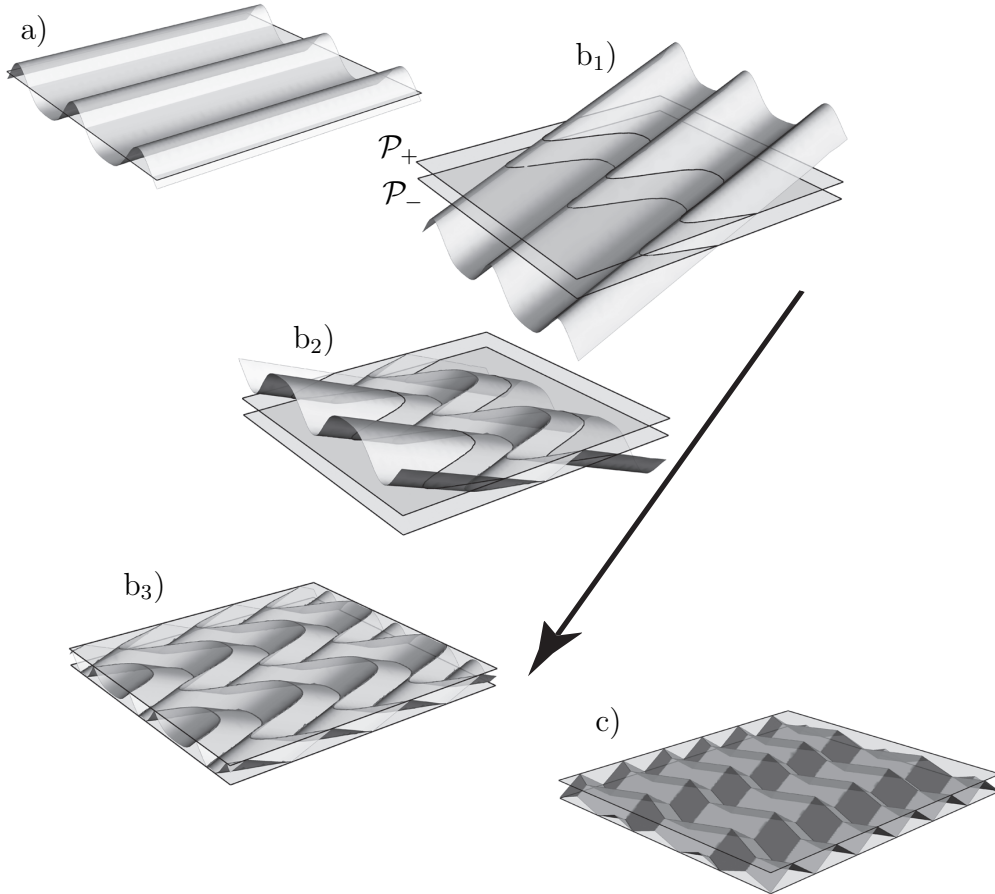
Fig. 2. Examples of developable surfaces representing film under large differential strain. (a) When the generatrices are parallel to the mean surface of the substrate, residual stress along the generatrices cannot be well relaxed. (b) When generatrices are tilted, repeated mirror symmetries allow the film to remain at a finite distance from the plane (Oxy). These symmetries create curvilinear ridges in general. (c) Particular case of a Miura-ori (piecewise straight ridges), studied in Section 4, obtained when the original cylindrical profile in (a) is generated by a sawtooth curve.

parallel to the mean plane of the film. Every other ridge lies in one of these planes. This construction defines a family of film shapes that are investigated in the rest of this paper.

Note that any surface similar to the one obtained in Fig. 2b$_3$ belongs to the quasi-one-dimensional class introduced in the simplified model of the companion paper (Audoly and Boudaoud, 2007b),

$$\mathcal{Q} = \{w(x,y) \mid w(x,y) = f(x - g(y))\}, \tag{9}$$

where $f(x)$ defines the film profile in a planar section, taken perpendicular to the mean direction of the crests and valleys ($f(x)$ is a sawtooth function in the present case), whereas $g(y)$ defines the profile of a crest or a valley along the plane $\mathcal{P}_+$ or $\mathcal{P}_-$ (this defines is another sawtooth function). It is not a

coincidence that Miura-ori pattern belong to the class $\mathcal{Q}$, as this class, introduced in the second paper, has been inspired by the results of the forthcoming Section 4 (with some anticipation).

Our goal is now to derive solutions of the equations given in Section 2 in the limit of large residual compression, based on the above construction. The developable surface just constructed makes the stretching energy of the film, in equation (3), vanish. However, the curvature diverges at the ridges and the bending energy is infinite there. This points to the existence of internal 'boundary layers' along the ridges. Such boundary layers were investigated by Pogorelov (1988) in the case of curvilinear ridges, and by Lobkovsky (1996) in the case of straight ridges. It was shown that straight ridges have in general a significantly lower energy than curvilinear ridges (see e.g. Pauchard and Rica, 1998) and we shall therefore start by comparing the energy of the two types of ridges in our system.

3.2 Smooth curvilinear ridges

We start by deriving the energy of the system when the ridges are curvilinear, as in Fig. 2b$_3$. We shall only need to estimate the order of magnitude of this energy as a function of the various parameters, and compare it to that for straight ridges: we drop prefactors of order unity in the present section and in the next one. A detailed analysis of the optimal network of folds, with all numerical factors included, is given in Section 4.

The film surface is periodic and is characterized by two wavelengths, one along the crests and valleys, and the other one across them. We assume that these two wavelengths are of the same order of magnitude λ, so that the area B of the unit cell of the periodic surface is of order $B \sim \lambda \times \lambda$. We consider developable surfaces, such that the strain $\epsilon_{\alpha\beta}$ vanishes. Then, by equation (8), the film slope appears to be of order $\sqrt{\eta}$, where η is the order of magnitude of the loading (η_x, η_y). As a result, the out-of-plane displacement can be estimated as $\tilde{w} \sim \lambda\sqrt{\eta}$.

We proceed to estimate the energy of the film. Pogorelov (1988) derived the energy of a curvilinear ridge having curvature $\kappa_{\mathrm{r}}(s)$ and dihedral angle $2\,\alpha(s)$ (the dihedral angle is defined as the arc cosine of the scalar products of the unit normals on either side of the ridge), where s is the curvilinear coordinate along the ridge:

$$\mathcal{U}_{\mathrm{cr}} = \frac{c_{\mathrm{cr}}\, E\, h^{5/2}}{[12\,(1-\nu^2)]^{3/4}} \int \kappa_{\mathrm{r}}^{1/2}(s)\, \alpha^{5/2}(s)\, \mathrm{d}s, \tag{10}$$

where $c_{\mathrm{cr}} \approx 1.2$ is a numerical prefactor.

8

A unit cell of area $B \sim \lambda^2$ contains two curvilinear ridges. Each ridge undulates with an amplitude of order λ and wavelength of order λ, hence a curvature $\kappa_{\mathrm{r}} \sim 1/\lambda$. The integral in equation (10) involves a total curvilinear length $\int \mathrm{d}s \sim \lambda$; the dihedral angle can be estimated as $2\alpha \sim \tilde{w}/\lambda \sim \sqrt{\eta}$. With these scalings, equation (10) yields the contribution of ridges to the film energy per unit surface as

$$\mathcal{E}_{\mathrm{f}}^{\mathrm{cr}} \sim \frac{\mathcal{U}_{\mathrm{cr}}}{B} \sim E\,h^{5/2}\,\eta^{5/4}\,\lambda^{-3/2}. \tag{11}$$

The energy of the elastic foundation (5) reads, for a typical wavenumber $\sim \pi/\lambda$ and deflection $\tilde{w}$:

$$\mathcal{E}_{\mathrm{s}} \sim E_{\mathrm{s}}\,\tilde{w}^2/\lambda \sim E_{\mathrm{s}}\,\lambda\,\eta. \tag{12}$$

The optimal wavelength of the pattern is obtained by minimizing the sum of film energy (11) and substrate energy (12). At minimum, the two energies are comparable. This yields, for the optimal wavelength:

$$\lambda \sim C^{2/5}\,h\,\eta^{1/10} \tag{13}$$

and for the total energy of the system:

$$\mathcal{E}_{\mathrm{t}}^{\mathrm{cr}} \sim E\,h\,C^{-3/5}\,\eta^{11/10}, \tag{14}$$

where C is the stiffness contrast of the film and substrate:

$$C = \frac{E}{E_s} \gg 1, \tag{15}$$

a large number by assumption.

In the analysis of the simplified model presented in the companion paper (Audoly and Boudaoud, 2007b), we found that the energy minimizers converge to developable surfaces. However, we derived a scaling $\mathcal{E}_{\mathrm{f}}^{\mathrm{approx}} \sim Eh^{7/3}\eta^{4/3}\lambda^{-4/3}$ for the energy of the film that differs from the exact one in equation (11) by a factor $\mathcal{E}_{\mathrm{f}}^{\mathrm{approx}}/\mathcal{E}_{\mathrm{f}}^{\mathrm{cr}} \sim (\tilde{w}/h)^{1/6}$, which is a large number in the limit we consider (large buckling number). Therefore, the curvilinear ridges investigated here have a lower energy than those found in the approximate model — recall that this model was based on the kinematical assumption $\mathcal{Q}$ defined in equation (9). This is because the structure of the ridge predicted by Pogorelov (1988) is not invariant along the ridge at small scales. For instance, the ridge width scales as $[h^{1/2}\,\kappa_{\mathrm{r}}^{-1/2}(s)\,\alpha^{1/2}]$, and so varies with s. As a result, the minimizers of the full model satisfy the kinematical condition $\mathcal{Q}$ far away from the ridges (as does the developable shape in Fig. 2b$_3$), but not very close to them. This discrepancy is not severe: the quasi-1D model overestimates the energy by a factor $(\tilde{w}/h)^{1/6}$ which grows very slowly with the buckling parameter, due to the small exponent $1/6$; for instance, when the deflection is three times the film thickness, the quasi-1D model overestimates the energy by no more than $\sim 20\ \%$.
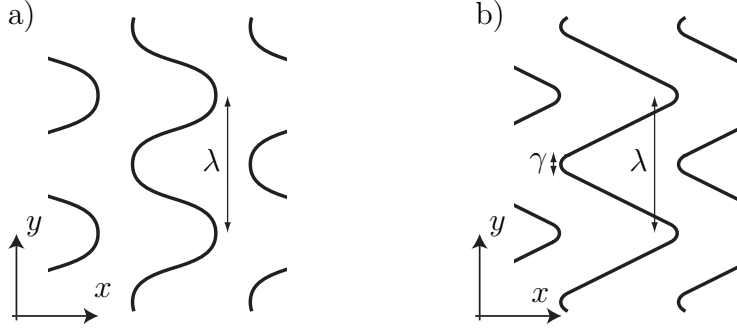
Fig. 3. Focusing of ridge curvature. (a) Smooth curvilinear ridges, as in Fig. 2b$_3$. (b) Focusing of curvature in a region of size γ much smaller than λ, leading to a herringbone (zigzag) pattern as in Fig. 2c.

3.3 Optimization of ridge profile: zigzag ridges

In the previous section, we studied the case when the ridges have smooth, rounded shapes, and the two wavelengths of the pattern and its amplitude are all comparable, of order λ. In the present section, we show that the optimal ridge shapes are in fact different: by focusing its curvature at sharp corners separated by straight segments, a ridge is able to decrease its energy by a large factor. As a result, the optimal ridge profiles are sawtooth-like, and not smooth.

Let us consider how the ridge energy (10) changes when the ridge goes to the sawtooth shape depicted in Fig. 3, right: the ridge profile is made of straight parts of edges $\sim \lambda$ connected by vertices having a spatial extent $\sim \gamma$, with $\gamma \ll \lambda$. In this situation, the curvature κ_r along the ridge vanishes everywhere, except at the angular points where it has a magnitude $\sim 1/\gamma$. By equation (10), the energy density associated with sawtooth-like ridges can then be estimated as

$$\frac{\mathcal{U}_{cr}}{B} \sim \frac{(E\,h^{5/2})\,\gamma^{-1/2}\,(\sqrt{\eta})^{5/2}\,\gamma}{\lambda^2} \sim (E\,h^{5/2}\,\eta^{5/4}\,\lambda^{-3/2})\left(\frac{\gamma}{\lambda}\right)^{1/2}.$$

In the first factor of the right-hand side, we have factored out the energy (11) for smooth ridges. Because of the second factor, the film energy becomes arbitrarily small when the curvature of the ridges focuses more and more ($\gamma/\lambda \to 0$). In fact, by adjusting the wavelength λ appropriately, it can be shown that both the film and the substrate energy (12) can be sent to zero in the limit $\gamma/\lambda \to 0$. This means that it is always optimal for the film energy to go from a smooth to a sawtooth-like ridge profile.

The present analysis, based on the theory of curvilinear ridges (Pogorelov, 1988), is not applicable to the straight part of the ridges, for which $\kappa_r = 0$ and so $\mathcal{U}_{cr} = 0$. It shows well that smooth ridges are not optimal (the energy is minimized when $\gamma \to 0$), but is unable to predict the small but nonzero value

10

of γ at equilibrium. The analysis of the optimal pattern, with zigzag ridges, has to be based on the solution of the plate equations for a *straight* ridge, derived by Lobkovsky, and not on that for curvilinear ridges. This is the aim of the next Section.

Note that the ridges of the simplified model derived in the second companion paper do not feature curvature focusing: we have shown both analytically and numerically that the function $g(y)$ converges to a sinusoid in the limit of large load (Audoly and Boudaoud, 2007b). This is again because the simplified model is unable to capture the details of the ridge structure at small scale. Despite this limitation, the simplified model is very useful as it provided a detailed account of the evolution of the pattern from undulating stripes at moderate strain to a piecewise smooth, periodic and developable surface at high compression.

3.4   Network of straight ridges

The previous arguments show that, among the family of developable surfaces introduced in Fig. 2, only those with straight ridges, such as in Fig. 2c, are potentially equilibrium solutions. In the rest of this paper, we analyze such solutions, called Miura-ori. We start by a scaling analysis of this pattern.

We consider film shapes given by Miura construction shown in Fig. 4, which is a periodic polyhedron obtained by patching parallelograms along their edges. The energy of a straight ridge depends only on its length ℓ and on the dihedral angle 2α between the neighboring facets (Lobkovsky et al., 1995; Lobkovsky, 1996):

$$\mathcal{U}_{\mathrm{sr}}(\ell, \alpha) = \frac{c_{\mathrm{sr}} \, E \, h^{8/3}}{[12 \, (1 - \nu^2)]^{5/6}} \; \ell^{1/3} \, \alpha^{7/3}, \tag{16}$$

where $c_{\mathrm{sr}} = 1.505$ is a numerical prefactor, as computed by Audoly and Pomeau (2008).

A unit cell of area $B \sim \lambda^2$ contains eight ridges of length $\ell \sim \lambda$. The associated dihedral angles scales as $\alpha \sim \sqrt{\eta}$, as earlier in Section 3.2. The energy of the film per unit surface then reads

$$\mathcal{E}_{\mathrm{f}}^{\mathrm{sr}} \sim \frac{\mathcal{U}_{\mathrm{sr}}}{B} \sim E \, h^{8/3} \, \lambda^{-5/3} \, \eta^{7/6}. \tag{17}$$

Note that this energy is smaller than the energy of smooth curvilinear ridges, given in equation (11), by a factor

$$\frac{\mathcal{E}_{\mathrm{f}}^{\mathrm{sr}}}{\mathcal{E}_{\mathrm{f}}^{\mathrm{cr}}} \sim \left(\frac{h}{\tilde{w}}\right)^{1/6}, \tag{18}$$

which is a very small number in the limit of a large buckling parameter, $\tilde{w} \gg h$. This confirms the argument of the previous section according to which straight ridges have a lower energy than smooth curvilinear ridges.

Minimizing the sum of the film energy $\mathcal{E}_{\mathrm{f}}^{\mathrm{sr}}$ in equation (17) and the substrate energy $\mathcal{E}_{\mathrm{s}}$ in equation (12) leads to the following scaling law for the wavelength:

$$\lambda \sim C^{3/8}\, \eta^{1/16}\, h, \tag{19}$$

while the total energy (per unit surface) becomes

$$\mathcal{E}_{\mathrm{t}}^{\mathrm{sr}} \sim E\, h\, C^{-5/8}\, \eta^{17/16}. \tag{20}$$

Having carried out the scaling analysis of the Miura-ori solution, we can now proceed to a detailed analysis of this pattern, including all numerical factors of order unity, which we have overlooked in a first approach.

4 Miura-ori solutions

In the present section, we extend the previous scaling analysis of a Miura-ori pattern to a quantitative analysis, and derive the energy of the pattern as a function of all the parameters of the problem. To do so, we first derive a parameterization of the film surface (Section 4.1), and compute the film energy based on a solution of the plate equations describing straight ridges (Section 4.2), and the substrate energy by computing the Fourier transform of the film profile (Section 4.3).

4.1 Film profile

At large buckling parameter, the film profile is a periodic developable surface with straight ridges, similar to the popular Miura-ori pictured in Fig. 4. This construction is made up of planar facets connected by straight ridges; it is a three dimensional tiling of identical parallelograms of width a and length b, with a skew angle θ. Before we give explicit formula for this profile, it is convenient introduce the sawtooth function with period 2 as follows

$$S(t) = \begin{cases} -1 - t & \text{if } -1 \leq t \leq -1/2, \\ t & \text{if } -1/2 \leq t \leq 1/2, \\ 1 - t, & \text{if } 1/2 \leq t \leq 1, \end{cases} \tag{21}$$

extended by periodicity for all t by $S(t+2) = S(t)$
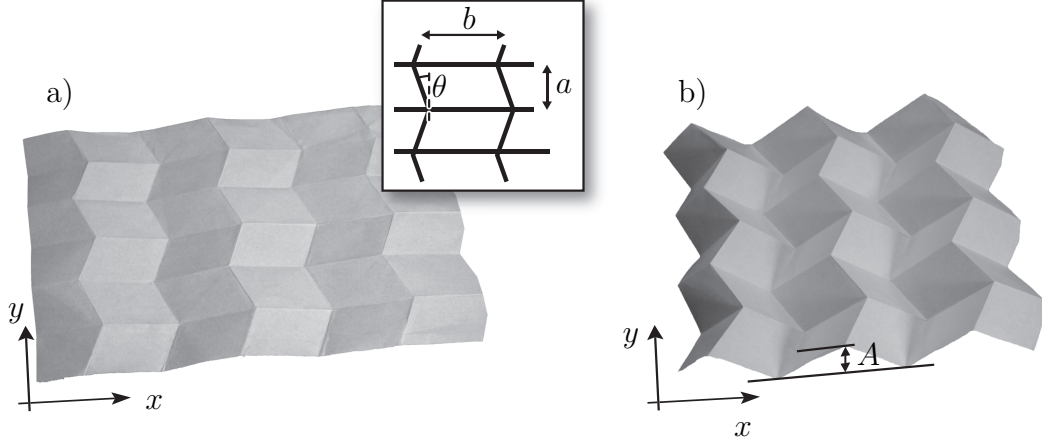
Fig. 4. Photographs of the Miura folding (Miura-ori) with a piece of paper. For any geometry of the network of ridges, given by the lengths a and b and the angle θ, this yields an articulated folded structure, parameterized by the transverse amplitude A.
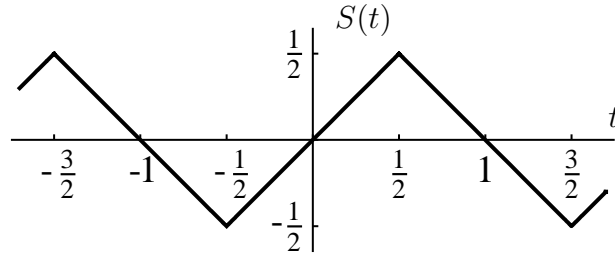
Fig. 5. Sawtooth function S defined by equation (21).

This function is plotted in Fig. 5.

The profile of the Miura-ori folding is most easily found in two steps. The first step is to remark that a section by a plane containing the x and z axes yields the sawtooth profile just introduced, up to scaling factors:

$$W(x) = w(x, y = 0) = A\,S\left(\frac{x}{b}\right), \tag{22}$$

where A is the amplitude of the pattern. In a second step, one notices that the surface is spanned by moving this 1D curve sideways along a zigzag path parallel to the crests and valleys. Such a zigzag path has the equation $x + a\,\tan\theta\left(\frac{1}{2} + S\left(\frac{y}{a} - \frac{1}{2}\right)\right) = C$, where C is a constant. This yields the following parameterization of the Miura-ori:

$$w(x, y) = W\left(x + a\,\tan\theta\left(\frac{1}{2} + S\left(\frac{y}{a} - \frac{1}{2}\right)\right)\right) \tag{23a}$$

$$= A\,S\left(\frac{x + a\,\tan\theta\left(\frac{1}{2} + S\left(\frac{y}{a} - \frac{1}{2}\right)\right)}{b}\right) \tag{23b}$$

13

This is the Cartesian equation of the Miura-ori profile shown in Fig. 4, right, with parameters a, b, θ, A.

We shall now work out the developability condition for a surface given by equation (23b). As explained earlier, the stretching is penalizing in the limit of large residual stress which we consider, and a necessary condition [2] for the energy to be minimum is $\epsilon_{\alpha\beta} = 0$. The in-plane displacement enters in the expression for the in-plane strain, but can be removed by considering the spatial averaging of Eqs. (2a-2c): the in-plane displacement u and v are bounded and their derivatives are zero on average. This yields:

$$0 = -\eta_x + \left\langle \frac{1}{2} \left(\frac{\partial w}{\partial x} \right)^2 \right\rangle$$

$$0 = -\eta_y + \left\langle \frac{1}{2} \left(\frac{\partial w}{\partial y} \right)^2 \right\rangle.$$

Here, the angular brackets stand for the spatial average of the quantity inside over the entire domain (x, y). Plugging the Miura-ori profile defined by equation (23b) into the two equations above, we find the developability condition:

$$\eta_x = \frac{1}{2} \left(\frac{A}{b} \right)^2 \tag{24a}$$

$$\eta_y = \frac{1}{2} \left(\frac{A \tan \theta}{b} \right)^2. \tag{24b}$$

These two equations relate some of the geometrical parameters, A, b and θ of the folding construction to the imposed differential strain. They can be used to eliminate A and θ:

$$A = b \sqrt{2\,\eta_x}, \qquad \tan \theta = \left(\frac{\eta_y}{\eta_x} \right)^{1/2}. \tag{25}$$

Using these relations, we shall consider from now on that the pattern is parameterized by a and b. In the following, we optimize the construction with respect to these main parameters, a and b.

Before we proceed, we note that the angle θ of the herringbone is given in equation (25) in terms of the ratio of η_y/η_x of principal strain values where, following our conventions, y denotes the average direction of the zigzag ridges forming the crests and valleys, although x is the direction of the family of ridges in the perpendicular direction, which go up and down. It can be easily

---

[2] The film profile is developable everywhere except in a very narrow region around of the folds. This effect, neglected here, would add a very small correction to the developability condition (24).

checked that equation (25) is a special case of the kinematic condition for developable surfaces belonging to the quasi-one-dimensional class $\mathcal{Q}$,

$$\langle g'^2 \rangle = \frac{\eta_y}{\eta_x},$$

derived in the companion paper (Audoly and Boudaoud, 2007b). Indeed for a sawtooth $g(y)$, the slope is $|g'| = \tan\theta$. The angle θ of the zigzags in equation (25) can be reexpressed in terms of the principal residual stress $(\sigma^0_{xx}, \sigma^0_{yy})$ using equation (1):

$$\tan^2\theta = (1 - \nu^2) \left(\frac{-\sigma^0_{xx}}{-\sigma^0_{yy}} - \nu \right)^{-1} - \nu \tag{26}$$

In the particular case of equi-biaxial compression, that is for $\eta_x = \eta_y$, or equivalently $\sigma^0_{xx} = \sigma^0_{yy}$, an important consequence of equation (25) is that

$$\theta = \frac{\pi}{4} \quad \text{(for equi-biaxial differential strain)}.$$

This explains that the chevrons patterns make kinks at right angles, as has been observed both in experiments (Bowden et al., 1998; Huck et al., 2000) and in numerical studies (Chen and Hutchinson, 2004; Huang et al., 2005).

4.2 Film energy

Our goal in the rest of this section is to derive, and then optimize, the energy of the pattern as a function of the remaining parameters a and b. The film is a polyhedron with planar facets, and the film energy resides in the ridges. The energy of an ridge has been given in equation (16) as a function of its length ℓ and of the dihedral angle 2α between the neighboring facets,

$$\mathcal{U}_{\text{sr}}(\ell, \alpha) = \frac{c_{\text{sr}} E h^{8/3}}{(12 (1 - \nu^2))^{5/6}} \, \ell^{1/3} \, \alpha^{7/3}, \tag{27}$$

Note that the following analysis does not depend crucially on the details of the formula above; any power-law dependence of the ridge energy on ℓ and α with positive exponents would yield similar results.

As can be seen from Fig. 4, two types of ridges are present in the Miura-ori, with lengths b and $a/\cos\theta$, and dihedral angles $2A\tan\theta/b$ and $2A/b\cos\theta$ respectively. The unit cell of the Miura-ori has an area $(4ab)$ and contains four ridges of each type. Therefore, the average energy of the film per unit surface

reads

$$\mathcal{E}_{\mathrm{f}}(a,b) = \frac{1}{4\,a\,b} \left(4\mathcal{U}_{\mathrm{sr}} \left(b, \frac{A\,\tan\theta}{b} \right) + 4\mathcal{U}_{\mathrm{sr}} \left(\frac{a}{\cos\theta}, \frac{A}{b\,\cos\theta} \right) \right). \qquad (28)$$

This provides an explicit formula for the film energy of the Miura-ori (herringbone) pattern.

4.3 Substrate energy

In order to determine the energy of the substrate, we first need to compute the Fourier coefficients of the vertical displacement $w(x,y)$ of the Miura-ori, given in equation (23b). To do so, we start with the Fourier expansion of the function associated with the curve $W(x) = w(x, y = 0)$ obtained by a planar section of the surface:

$$W(x) = \sum_{k'=0}^{\infty} W_{k'}\,\sin(\nu_{k'}\,x),$$

$$\text{where} \quad W_{k'} = (-1)^{k'} \frac{4\,A}{\pi^2\,(2k'+1)^2} \text{ and } \nu_{k'} = \frac{\pi}{b}\,(2k'+1).$$

Then, using the definition (23b) of $w(x,y)$, and introducing the C^∞ smooth functions $\operatorname{sinc} u = \sin u/u$ and $\operatorname{cosc} u = (1 - \cos u)/u$, we obtain

$$w(x,y) = \frac{1}{2} \sum_{k=0,k'=0}^{\infty} \Big(W_{k'}\,s_{k,k'}\,\cos(\lambda_k y + \nu_{k'} x) + W_{k'}\,s_{k,k'}\,\cos(\lambda_k y - \nu_{k'} x)$$

$$+ W_{k'}\,c_{k,k'}\,\sin(\lambda_k y + \nu_{k'} x) + W_{k'}\,c_{k,k'}\,\sin(\lambda_k y - \nu_{k'} x) \Big)$$

where

$$s_{k,k'} = \operatorname{cosc}\left((\lambda_k + \nu'_k \tan\theta)\,a \right) + \operatorname{cosc}\left((\nu'_k \tan\theta - \lambda_k)\,a \right),$$
$$c_{k,k'} = \operatorname{sinc}\left((\lambda_k + \nu'_k \tan\theta)\,a \right) + \operatorname{sinc}\left((\nu'_k \tan\theta - \lambda_k)\,a \right),$$
$$\lambda_k = \frac{\pi}{a}\,k,$$

and k and k' are integers indexing the Fourier modes.

The substrate energy (5) per unit surface can then be written as

$$\mathcal{E}_{\mathrm{s}}(a,b) = \frac{E^*}{8} \sum_{k,k'} \frac{W_{k'}^2}{1 + \delta_0^k} \sqrt{\lambda_k^2 + \nu_{k'}^2}\,\left(s_{k,k'}^2 + c_{k,k'}^2 \right). \qquad (29)$$

The Kronecker symbol is defined by $\delta_0^k = 1$ if $k = 0$, and $\delta_0^k = 0$ otherwise.

16

4.4 Energy minimization

The total energy, to be minimized, is the sum of the film and substrate energies, given in equations (28) and (29) respectively. In order to put the equations in dimensionless form, we introduce the aspect ratio

$$\rho = \frac{a}{b},$$

and the typical length a^* and energy $\mathcal{E}^*$,

$$a^* = \left(\frac{c_{\mathrm{sr}}\, E}{(12\,(1-\nu^2))^{5/6}\, E_{\mathrm{s}}^*} \right)^{3/8} (2\,\eta_x)^{1/16}\, h \quad \text{and} \quad \mathcal{E}^* = 2\,\eta_x\, E_{\mathrm{s}}^*\, a^*.$$

Introducing the rescaled length $\overline{a} = a/a^*$, the total energy $\mathcal{E}_{\mathrm{t}}(a,b) = \mathcal{E}_{\mathrm{f}}(a,b) + \mathcal{E}_{\mathrm{s}}(a,b)$ takes the dimensionless form

$$\frac{\mathcal{E}_{\mathrm{t}}(\overline{a},\rho)}{\mathcal{E}^*} = \left(\frac{\overline{a}}{\rho^2}\, \overline{\mathcal{U}_{\mathrm{s}}}(\rho,\theta) + \frac{\rho}{\overline{a}^{5/3}}\, \overline{\mathcal{U}_{\mathrm{f}}}(\rho,\theta) \right), \tag{30}$$

where the functions

$$\overline{\mathcal{U}_{\mathrm{f}}}(\rho,\theta) = 2^{7/3} \left(\frac{\tan^{7/3}\theta}{\rho^{1/3}} + \frac{1}{\cos^{8/3}\theta} \right) \tag{31a}$$

$$\overline{\mathcal{U}_{\mathrm{s}}}(\rho,\theta) = \frac{\rho^2}{E_{\mathrm{s}}a}\mathcal{E}_{\mathrm{s}}(a,b) \tag{31b}$$

are known numerical functions depending the aspect ratio ρ and on the angle θ only. The function $\overline{\mathcal{U}_{\mathrm{s}}}(\rho,\theta)$ is not given here for the sake of brevity but it can easily be found from equation (29).

Returning to the optimization problem, we first minimize the total energy $\mathcal{E}_{\mathrm{t}}(\overline{a},\eta)$ with respect to the rescaled dimension of the pattern, $\overline{a}$. The condition $\partial \mathcal{E}_{\mathrm{t}}/\partial \overline{a} = 0$ yields

$$\overline{a}(\rho) = \left(\frac{5\,\rho^3}{3} \frac{\overline{\mathcal{U}_{\mathrm{f}}}(\rho)}{\overline{\mathcal{U}_{\mathrm{s}}}(\rho)} \right)^{3/8}, \tag{32a}$$

and the energy becomes a function of the parameter ρ only:

$$\mathcal{E}_{\mathrm{t}}^{\dagger}(\rho) \equiv \min_{\overline{a}} \mathcal{E}_{\mathrm{t}}(\overline{a},\rho) = \frac{8\,\mathcal{E}^*}{5} \frac{\overline{a}(\rho)\,\overline{\mathcal{U}_{\mathrm{s}}}(\rho)}{\rho^2} \tag{32b}$$

There remains to optimize with respect to the pattern aspect ratio ρ. The reduced energy $\mathcal{E}_{\mathrm{t}}^{\dagger}(\rho)$ is plotted in Fig. 6 in the case of equi-biaxial compression ($\theta = \pi/4$). It appears to be a monotonically decreasing function: the optimum is reached for an infinite aspect ratio $\rho = a/b \to \infty$. It is not possible to select a well-defined Miura-ori pattern by energy minimization.
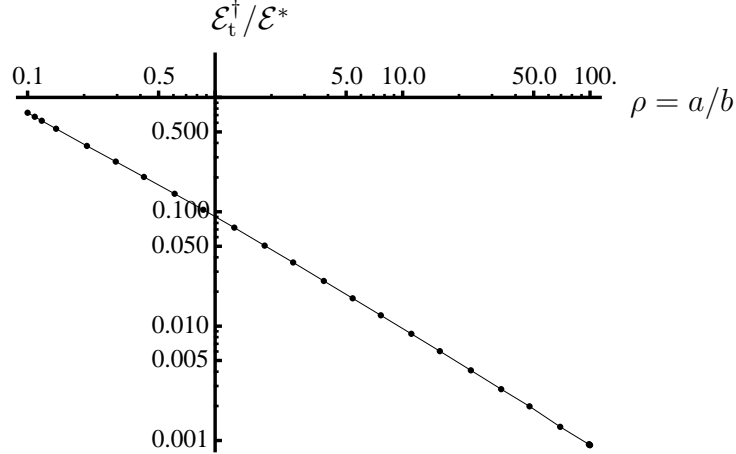
Fig. 6. Log-log plot of the reduced energy (32b) of the Miura-ori pattern as a function of the aspect ratio $\rho = a/b$ in the case of equi-biaxial compression ($\theta = \pi/4$). The optimal choice is $\rho \to \infty$, that is $a \gg b$.

The fact that a large aspect ratio ρ is energetically favorable can be understood as follows. According to equation (5), the substrate energy associated with a pure Fourier mode with wavevector $(\nu_{k'}, \lambda_k)$ goes like $|(\nu_{k'}, \lambda_k)| A^2$. In the limit $\rho = a/b \gg 1$, the dominant contribution to the norm of this wavevector comes from the y component since $\lambda_k \propto 1/b$ although $\nu_{k'} \propto 1/a$. For a large aspect ratio, the substrate energy is therefore dominated by the small scale perturbation, at scale b, and is of order $\mathcal{E}_s(a,b) \sim E_s^* A^2/b$. Using the kinematical relation (24a), this yields $\mathcal{E}_s \sim E_s^* b \eta_x$. On the other hand, the long ridges, of length a, make a dominant contribution to the film energy. As a result, the film energy scales as $\mathcal{E}_f(a,b) \sim Eh^{8/3}a^{1/3}(A/b)^{5/3} \sim Eh^8/3(\eta_x)^{7/6}a^{-2/3}b^{-1}$. As a result, it is possible to make both energy contributions go to zero at fixed differential strain, by taking $b \to 0$ while $a^{2/3}b \to \infty$.

4.5   Trapping

In the limit of large differential strain, the absolute minimum of energy of the system is reached when the Miura-ori pattern has an infinite aspect ratio. This corresponds to a series of stripes organized in chevrons, such that the stripe spacing is much smaller than the distance between angular points. This is very similar with the results obtained with a simplified buckling model in the companion paper (Audoly and Boudaoud, 2007b): we found that the absolute minimum of energy corresponds to a pattern made of a series of undulating stripes that are very close from each other.

In experiments where herringbones have been observed, the two wavelengths of the pattern, namely the stripes spacing and the distance between kinks, appear to be comparable. This points to the fact that the wavelengths are not

18

selected by energy minimization. Indeed, as shown by analysis and the numerical simulations of the simplified model (Audoly and Boudaoud, 2007b), the observed wavelengths depend on the history of the loading. Under increasing load, the system remains trapped in a metastable equilibrium having two comparable wavelengths, determined by the primary and secondary buckling bifurcations.

5   Conclusion

We have studied the buckling of a thin film bound to a compliant substrate. We derived analytical solutions of this problem in the limit of large residual stress (strongly post-buckled limit). We started by introducing a family of developable solutions, relevant to this limit, obtained by repeatedly patching pieces of a cylindrical surface along ridges. In general, these ridges can be curvilinear but we have shown that the elastic energy is minimum when the ridge curvature concentrates. This provides a simple interpretation for 'herringbone' patterns reported in experiments under approximately equi-biaxial compression by Bowden et al. (1998) and Huck et al. (2000), and in the finite elements simulations of a unit cell of a periodic pattern by Chen and Hutchinson (2004).

In herringbone patterns, the crests and valleys follow a set of parallel sawtooth-like curves. We derived a robust geometrical result, namely that the kink angle (2θ) of these curves is directly related to the ratio of the principal residual compressive stresses, see equation (26). In the particular case of equi-biaxial loading, the crests and valleys must kink at right angle, which is consistent with previous experimental and numerical observations (see Chen and Hutchinson (2004) in particular).

Making full use of the similarity of this pattern with a popular origami folding (Miura-ori), we have expressed the film deflection as a function of the wavelengths and other geometrical parameters. We derived a closed-form expression for the energy of the pattern as a function of these parameters, in the limit of large load. We found that this energy is at its absolute minimum when the aspect ratio of the pattern, defined as the ratio of the crests' zigzag wavelength to the gap between crests, becomes infinite. However, the simplified buckling model studied in the companion paper (Audoly and Boudaoud, 2007b), reveals that the wavelengths observed under monotonically increasing loading are not those with the absolute lowest energy: the system is trapped in a local minimum of energy and the pattern aspect ratio, determined once for all by the primary and secondary bifurcations, remains of order one even at large load. This is consistent with the experimental observation that the longitudinal wavelength of the zigzags is comparable with the gap between them, both

being close to the wavelengths predicted by the primary and secondary buckling instabilities. Moreover, the present analysis reveals the existence of many metastable states and this may explain the variability of patterns observed in the experiments.

This paper closes a set of papers analyzing buckling of a stiff plate under compressive residual stress, and bonded to a compliant substrate. Straight stripes have been well studied and are known to appear above a (primary) buckling threshold. In part I, we investigated the limit of small load, and showed that secondary buckling instabilities lead to checkerboard patterns for equi-biaxial loading and to undulating stripes for biaxial (but not equi-biaxial) loading. In part II, we proposed a global scenario for the evolution from undulating stripes to herringbones as the loading is gradually increased. In part III (the present one), we derived an asymptotic solution describing herringbone patterns in the limit of a large buckling parameter. We have used a variety of mathematical methods, from a classical analysis of stability, to weakly and strongly non-linear post-buckling analyses. An unusual feature of the primary and secondary buckling bifurcations comes from non-linear interactions between the classical buckling modes, which eventually yield complex patterns. In the strongly post-buckled regime, developable solutions have been obtained by an asymptotic analysis. For intermediate load, no exact solution is available and a buckling model based on carefully chosen approximations allowed us to put all results in a consistent framework. We believe that the methods used here should be applicable to many other buckling problems.

Even though the geometry of a thin elastic plate bonded to a compliant substrate is particularly simple, it can lead to many different buckling patterns depending on the loading conditions; we encountered straight and undulating stripes, varicose, hexagonal, checkerboard and herringbone patterns. The labyrinthine one, observed by Bowden et al. (1998) and many others, has remained unexplained to date — we may conjecture that this aperiodic pattern follows from a superposition of an infinite number of the classical, cylindrical buckling modes.

References

Allen, H. G., 1969. *Analysis and Design of Structural Sandwich Panels.* Pergamon Press, New York.

Audoly, B., Boudaoud, A., 2007a. Buckling of a thin film bound to a compliant substrate (part I). Formulation, linear stability of cylindrical patterns, secondary bifurcations. Submitted to Journal of the Mechanics and Physics of Solids.

Audoly, B., Boudaoud, A., 2007b. Buckling of a thin film bound to a compli-

ant substrat (part II). A global scenario for the formation of herringbone pattern. Submitted to Journal of the Mechanics and Physics of Solids.

Audoly, B., Pomeau, Y., 2008. *Elasticity and geometry: from hair curls to the nonlinear response of shells.* Oxford University Press.

Ben Amar, M., Pomeau, Y., 1997. Crumpled paper. Proceedings of the Royal Society A: Mathematical, Physical and Engineering Sciences 453, 729–755.

Bowden, N., Brittain, S., Evans, A. G., Hutchinson, J. W., Whitesides, G. M., 1998. Spontaneous formation of ordered structures in thin films of metals supported on an elastomeric polymer. Nature 393, 146–149.

Chen, X., Hutchinson, J. W., 2004. Herringbone buckling patterns of compressed thin films on compliant substrates. Journal of Applied Mechanics 71, 597–603.

Choksi, R., Kohn, R. V., Otto, F., 1999. Domain branching in uniaxial ferromagnets: A scaling law for the minimum energy. Communications in Mathematical Physics 201, 61—79.

Conti, S., 2000. Branched microstructures: scaling and asymptotic self-similarity. Communications on Pure and Applied Mathematics 53, 1448–1474.

Genzer, J., Groenewold, J., 2006. Soft matter with hard skin: from skin wrinkles to templating and material characterization. Soft Matter 2, 310–323.

Huang, Z. Y., Hong, W., Suo, Z., 2005. Nonlinear analyses of wrinkles in a film bonded to a compliant substrate. Journal of the Mechanics and Physics of Solids 53, 2101–2118.

Huck, W., Bowden, N., Onck, P., Pardoen, T., Hutchinson, J., Whitesides, G., 2000. Ordering of spontaneously formed buckles on planar surfaces. Langmuir 16, 3497–3501.

Jin, W., Sternberg, P., 2001. Energy estimates for the von Kàrmàn model of thin-film blistering. Journal of Mathematical Physics 42, 192–199.

Libai, A., Simmonds, J. G., 1998. *The nonlinear theory of elastic shells.* Cambridge University Press, 2nd edn.

Lobkovsky, A., Gentges, S., Li, H., Morse, D., Witten, T. A., 1995. Scaling properties of stretching ridges in a crumpled elastic sheet. Science 270, 1482–1485.

Lobkovsky, A. E., 1996. Boundary layer analysis of the ridge singularity in a thin plate. Physical Review E (Statistical, Nonlinear, and Soft Matter Physics) 53, 3750–3759.

Mahadevan, L., Rica, S., 2005. Self-organized origami. Science 307, 1740.

Miura, K., 1980. Method of packaging and deployment of large membranes in space. In: *Proceedings of 31st IAF Congress*, Springer-Verlag, ed., Paper no IAF–80–A31. Tokyo.

Pauchard, L., Rica, S., 1998. Contact and compression of elastic spherical shells: the physics of a 'ping-pong' ball. Phil. Mag. B 78, 225–233.

Pogorelov, A. V., 1988. *Bendings of surfaces and stability of shells.* No. 72 in Translation of mathematical monographs. American Mathematical Society.

Pomeau, Y., Rica, S., 1997. Plaques très comprimées. Comptes Rendus

de l'Académie des Sciences - Series IIB - Mechanics-Physics-Chemistry-Astronomy 325, 181–187.

Spivak, M., 1979. *A comprehensive introduction to differential geometry*, vol. 5. Publish or perish, Inc., Houston (TX), 2nd edn.

Timoshenko, S., Gere, J. M., 1961. *Theory of elastic stability.* MacGraw Hill, New York, 2nd edn.

Yoo, P. J., Suh, K. Y., Park, S. Y., Lee, H. H., 2002. Physical self-assembly of microstructures by anisotropic buckling. Advanced materials 14, 1383–1387.